

Is 2D Heatmap Representation Even Necessary for Human Pose Estimation?

Yanjie Li^{*1,2} Sen Yang^{*2,3} Shoukui Zhang² Zhicheng Wang^{†2}
 Wankou Yang³ Shu-Tao Xia^{†1,4} Erjin Zhou²

¹Tsinghua University ²MEGVII Technology ³Southeast University
⁴PCL Research Center of Networks and Communications, Peng Cheng Laboratory
 lyj20@mails.tsinghua.edu.cn yangsenius@seu.edu.cn
 {zhangshoukui, wangzhicheng}@megvii.com
 wkyang@seu.edu.cn xiast@sz.tsinghua.edu.cn zej@megvii.com

Abstract

The 2D heatmap representation has dominated human pose estimation for years due to its high performance. However, heatmap-based approaches have some drawbacks: 1) The performance drops dramatically in the low-resolution images, which are frequently encountered in real-world scenarios. 2) To improve the localization precision, multiple upsample layers may be needed to recover the feature map resolution from low to high, which are computationally expensive. 3) Extra coordinate refinement is usually necessary to reduce the quantization error of downsampled heatmaps. To address these issues, we propose a **Simple** yet promising **Disentangled Representation** for keypoint coordinate (*SimDR*), reformulating human keypoint localization as a task of classification. In detail, we propose to disentangle the representation of horizontal and vertical coordinates for keypoint location, leading to a more efficient scheme without extra upsampling and refinement. Comprehensive experiments conducted over COCO dataset show that the proposed *heatmap-free* methods outperform *heatmap-based* counterparts in all tested input resolutions, especially in lower resolutions by a large margin. Code will be made publicly available at <https://github.com/leeyegy/SimDR>.

1 Introduction

2D human pose estimation (HPE) aims to localize body joints from a single image. Prevalent methods always adopt the encoder-decoder pipeline to estimate the keypoints location. Most methods adopt deep convolutional neural network (CNN) as feature encoder owing to its great performance. In terms of the decoder part, existing approaches fall into two broad categories: *heatmap-based* [2, 3, 5, 6, 40, 16, 17, 19, 22, 29, 37, 38] and *regression-based* [34, 15, 31, 20, 32, 15] methods. The former is adopted in most cases.

Directly regressing the numerical coordinates of joints [34, 32, 15] is the most straightforward way to locate keypoints. Numerical regression tends to be simple and computationally friendly. Nevertheless, it lacks spatial generalization, resulting in inferior predictions in most tough cases.

The alternative is to encode joint coordinates into 2D heatmaps. Owing to its remarkable performance in unconstrained situations, the heatmap-based pipeline has naturally become the *de facto* standard label representation for HPE. In detail, heatmap is generated as a 2-dimensional Gaussian distribution centering at the ground-truth joint position. Heatmap-based coordinate representation inhibits the

^{*}This work was done when Yanjie and Sen Yang were interns at MEGVII Tech.

[†]Correspondence to: Shu-Tao Xia and Zhicheng Wang.

Table 1: Comparisons between *heatmap* and the proposed *SimDR*. H and W mean the height and width of the input image respectively. λ is the downsampling ratio, which is often set as 4. $k(\geq 1)$ is the splitting factor.

	Heatmap	SimDR
Representation complexity	$O(H \times W)$	$O(H + W)$
No need of coordinate refinement	✗	✓
Good for low-res input	✗	✓
Good for high-res input	✓	✓
Quantisation error	$[0, \frac{\lambda}{2}]$	$[0, \frac{1}{2k}]$

cases of false positive and makes the training process smoother by assigning a probability (uncertainty) value to each position, thus achieving significant improvement over regression-based methods.

However, heatmap-based methods suffer from several shortcomings. First, to output the 2D heatmaps, costly upsampling operations (e.g., deconvolution layers in [37]) are always necessary. Second, to alleviate the projecting errors from heatmap to ground truth (GT) coordinates, extra post-processing is inevitable to further refine the results. Last but not least, the performances of heatmap-based methods usually drop sharply as the input resolution decreases. For instance, we observe that the performance of HRNet-W48 [29] drops surprisingly from 75.1 AP to 48.5 AP when degrading the input resolution from 256×192 to 64×64 . The advantage of heatmap-based method tends to be concealed by its quantization error in low input resolution cases, resulting in inferior performance.

Therefore, we raise the question: *is the 2D heatmap representation that jointly encodes horizontal and vertical keypoint coordinates necessary for sustaining superior performance?*

We are inspired by the recent Transformer-based human pose estimation methods [17, 38], which also adopt 2D heatmap as the output. However, different from typical Fully Convolutional Network (FCN) architectures, they do not consistently keep the 2D structure of feature maps through the whole pipeline. Particularly, TokenPose [17] uses a shared MLP to predict 2D heatmaps, where each type of keypoint heatmap is transformed from a keypoint token (1D vector). Also, [7] proposes compressed volumetric heatmaps that can encode multi-person keypoints' positions in a compressed code and recover their positions by a decoder. These findings indicate that the heatmap representation with explicit spatial structure may not be a necessity to encode position information.

In order to further explore the efficiency of keypoint representation, we propose a novel approach named Simple Disentangled coordinate Representation (*SimDR*) for human pose estimation. *SimDR* encodes the (x, y) coordinate of keypoint into two independent 1D vectors with the same or higher quantization level w.r.t. the original image. The comparisons between different coordinate representation schemes are shown in Figure 1.

We apply *SimDR* to the typical CNN-based or Transformer-based human pose estimation models and achieve superior results in contrast to the 2D heatmap representation under various input resolution conditions, particularly, the low-resolution input. We hope this simple baseline could motivate the community to rethink the design of coordinate representation for 2D human pose estimation. Our contributions are summarized as follows:

- We propose a novel keypoint position representation, which disentangles the representation of x - and y - coordinate of keypoint into two independent 1D vectors. It regards the keypoint localization task as two sub-tasks of classification at horizontal and vertical directions. The advantages of our method over heatmap-based methods are presented in Table 1.
- The proposed *SimDR* allows one to remove the time-consuming upsampling module of some methods. Applying *SimDR* and removing the deconvolution module largely reduce over 55% GFLOPs of SimBa-Res50 [37] and achieve higher model performance (see Table 4).
- Comprehensive experiments are conducted over three datasets: COCO keypoint detection dataset [18], CrowdPose [14] and MPII [1]. For the first time, the proposed *SimDR* brings *heatmap-free* methods to the competitive performance level of *heatmap-based* methods, outperforming the latter by a large margin in low input resolution cases.

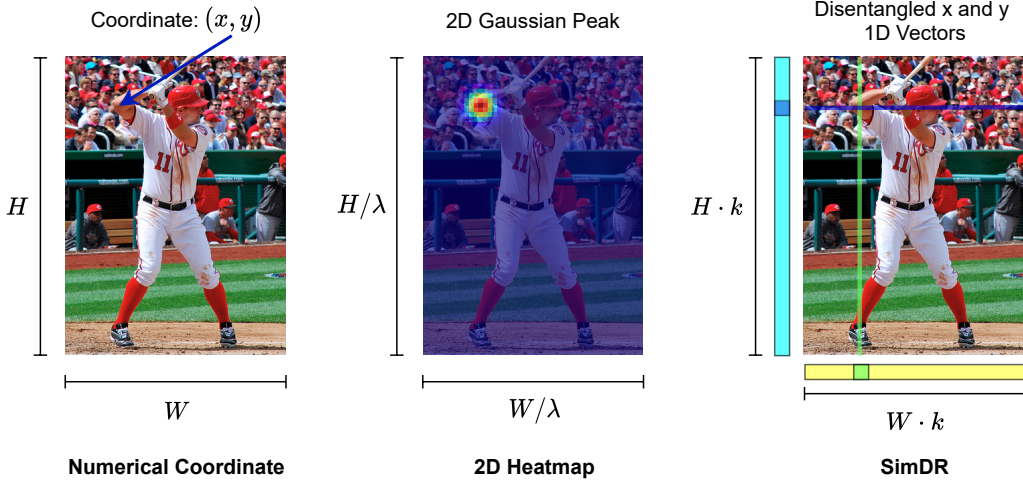


Figure 1: The comparisons between different coordinate representation schemes. H, W are the height and width of the original input image. $\lambda (\in \{1, 2, 4, \dots\})$ is the downsampling ratio for the 2D heatmap, which is often set as 4 in prevalent methods like SimpleBaseline [37], Hourglass [22], or HRNet [29]. $k (\geq 1)$ is the splitting factor for SimDR.

2 Related Work

Regression-based methods. Regression-based methods [34, 4, 32, 31, 30, 24, 15, 20] are explored in the early stage of 2D human pose estimation. Different from relying on 2D grid-like heatmap, this line of work directly regresses the keypoint coordinates in a computationally friendly framework. However, regression-based methods lack the ability of spatial generalization [23]. As a result, there is a huge gap between regression-based and heatmap-based methods, which limits the practical application of it.

Heatmap-based methods. Another line of work [2, 3, 5, 6, 16, 17, 19, 22, 29, 37, 38, 40] adopts two-dimensional Gaussian distribution (i.e., *heatmap*) to represent joint coordinate. Each position on the heatmap is assigned with a probability to be the ground truth point. As one of the earliest uses of heatmap, Tompson et al. [33] propose a hybrid architecture consisting of a deep Convolutional Network and a Markov Random Field. Newell et al. [22] introduce hourglass-style architecture into HPE. Papandreou et al. [26] propose to aggregate the heatmap and offset prediction to improve the localization precision. Xiao et al. [37] propose a simple baseline that utilizes three deconvolutional layers following a backbone network to obtain the final predicted heatmap. Instead, Sun et al. [29] propose a novel network to maintain high-resolution representations through the whole process, achieving significant improvement. Moreover, Zhang et al. [40] introduce distribution-aware coordinate representation to deal with the quantization error of downscaled heatmaps. Owing to the involvement of spatial uncertainty, this kind of learning schema has the tolerance of mistakes of jitter. False positives are alleviated when the coordinate migration refinement is engaged as post-processing. As a result, heatmap-based methods keep stable state-of-the-art performance for years. However, quantization error remains a significant problem of the heatmap-based methods, especially, in low input resolutions. In addition, extra post-processing is complex and costly in practical deployment scenarios. By contrast, the proposed SimDR properly settles the these issues and obtains remarkable improvements in various input resolutions.

3 Method

In this section, we firstly revisit the heatmap-based coordinate representation. Then, we illustrate the proposed Simple Disentangled coordinate Representation (SimDR) for human keypoint coordinate. In this paper, we mainly focus on the top-down paradigm of multi-person pose estimation.

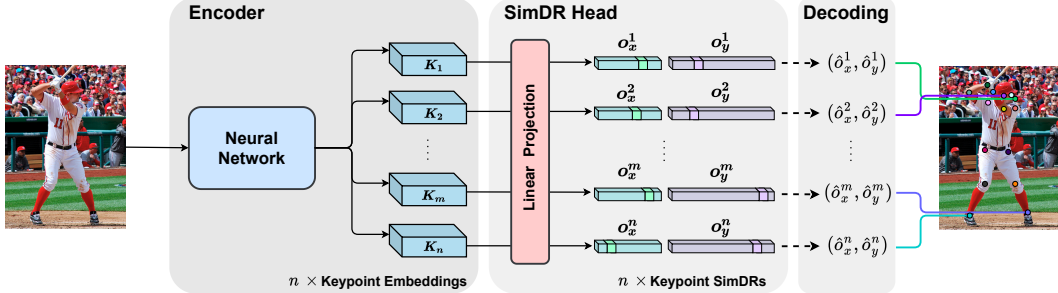


Figure 2: The schematic diagram of combining the SimDR with a given neural network. When using a neural network like SimpleBaseline or HRNet as the encoder, the keypoint embeddings, $\{\mathbf{K}_i\}_{i=1}^n$ ($\mathbf{K}_i \in \mathbb{R}^d$), are achieved by rearranging the shape of feature maps into $n \times d$, where n is the number of keypoint types. Then, the SimDR head, a shared linear projection layer, transforms each embedding into two 1D vectors ($\mathbf{o}_x^i, \mathbf{o}_y^i$) whose lengths are $W \cdot k$ and $H \cdot k$.

3.1 Heatmap-based Coordinate Representation

As the *de facto* standard coordinate representation in human pose estimation, *heatmap* adopts spatial confidence distribution to represent the keypoint coordinates. The resulted heatmap is designed to follow a 2D Gaussian distribution:

$$G(\mathbf{m}; \boldsymbol{\mu}, \Sigma) = \frac{1}{2\pi|\Sigma|^{\frac{1}{2}}} \exp\left(-\frac{1}{2}(\mathbf{m} - \boldsymbol{\mu})^T \Sigma^{-1} (\mathbf{m} - \boldsymbol{\mu})\right) \quad (1)$$

where \mathbf{m} is a pixel of the heatmap in the position (m_x, m_y) , $\boldsymbol{\mu}$ is the target joint location. Σ is a pre-defined diagonal covariance matrix.

Note that each of the outputted heatmaps represents the spatial distribution of one specific keypoint. The final coordinates are obtained by the maximum indices of the predicted heatmaps.

3.2 SimDR: Reformulating the Localization from the Perspective of Classification

In SimDR, x - and y - coordinates are disentangled into 1D vectors respectively instead of being jointly encoded.

Coordinate encoding. Given an input image of size $H \times W \times 3$, we denote the ground-truth coordinate for the p -th type of keypoint as (x^p, y^p) . To enhance the precision of localization, we introduce a splitting factor $k (\geq 1)$ and rescale the ground-truth coordinate into a new coordinate³:

$$\mathbf{p}' = (x', y') = (\text{round}(x^p \cdot k), \text{round}(y^p \cdot k)), \quad (2)$$

where $\text{round}(\cdot)$ is a round function. This splitting factor can enhance the localization precision to the level of *sub-pixel*. Furthermore, the supervision signals are defined as:

$$\mathbf{p}'_x = [x_0, x_1, \dots, x_{W \cdot k - 1}] \in \mathbb{R}^{W \cdot k}, x_i = \mathbb{1}(i = x'), \quad (3)$$

$$\mathbf{p}'_y = [y_0, y_1, \dots, y_{H \cdot k - 1}] \in \mathbb{R}^{H \cdot k}, y_j = \mathbb{1}(j = y'), \quad (4)$$

where $i \in \{0, 1, \dots, W \cdot k - 1\}$, $j \in \{0, 1, \dots, H \cdot k - 1\}$. $\mathbb{1}(\cdot)$ means indicator function. Both \mathbf{p}'_x and \mathbf{p}'_y are 1D vectors.

Coordinate decoding. Assuming the model outputs two 1D vectors \mathbf{o}_x and \mathbf{o}_y for a given type of keypoint, the final predicted absolute joint position (\hat{o}_x, \hat{o}_y) is calculated by:

$$\hat{o}_x = \frac{\arg \max_i (\mathbf{o}_x(i))}{k}, \hat{o}_y = \frac{\arg \max_j (\mathbf{o}_y(j))}{k}. \quad (5)$$

This reduces the quantization error from the level $[0, \frac{\lambda}{2}]$ of the $\lambda \times$ downsampled heatmap to the level $[0, \frac{1}{2k}]$. See Appendix D for details.

³We omit the superscript p for brevity.

Network Architecture. As shown in Figure 2, the SimDR representation requires the neural architecture to output n keypoint embeddings (n is the number of keypoint types) and to append a linear layer to project each keypoint embedding into two length-fixed 1D vectors. So this method can be combined with any common CNN-based or Transformer-based neural networks which can learn powerful feature representation.

Training Targets and Loss function. Considering SimDR treats the task of keypoint localization as a kind of classification task, the general classification loss functions can be exploited instead of the mean square error (MSE) loss used in 2D heatmap representation. Naively, we use the cross-entropy loss to train the models⁴.

3.3 Advanced Space-aware SimDR

It seems that SimDR illustrated above treats the false labels equally, which has ignored the spatial relevance of adjacent labels for the task of keypoint localization. To address this issue, we propose an advanced variant of SimDR, denoted as SimDR*, which generate the supervision signals in a space-aware way:

$$\mathbf{p}'_{\mathbf{x}_{sa}} = [x_0, x_1, \dots, x_{W \cdot k - 1}] \in \mathbb{R}^{W \cdot k}, x_i = \frac{1}{\sqrt{2\pi}\sigma} \exp\left(-\frac{(i - x')^2}{2\sigma^2}\right), \quad (6)$$

$$\mathbf{p}'_{\mathbf{y}_{sa}} = [y_0, y_1, \dots, y_{H \cdot k - 1}] \in \mathbb{R}^{H \cdot k}, y_j = \frac{1}{\sqrt{2\pi}\sigma} \exp\left(-\frac{(j - y')^2}{2\sigma^2}\right), \quad (7)$$

where σ is the standard deviation. And we use Kullback–Leibler divergence for model training.

4 Experiments

In the following sections, we empirically investigate the effectiveness of the proposed SimDR for 2D human pose estimation. We conduct experiments on three benchmark datasets: COCO [18], CrowdPose [14], and MPII [1]. The results on CrowdPose and MPII are presented in Appendix.

4.1 COCO Keypoint Detection

As one of the largest and most challenging datasets for HPE, the COCO dataset [18] contains more than 200,000 images and 250,000 person instances labeling with 17 keypoints (e.g., nose, left ear, etc.). The COCO dataset is divided into three parts: 57k images for the training set, 5k for val set and 20k for test-dev set. Note that all the methods reported in this paper are trained only on the train2017 set and evaluated on the val2017 set and test-dev2017 set. In this paper, we follow the data augmentation in [29].

Evaluation metric. The standard average precision (AP) is used as our evaluation metric on the COCO dataset, which is calculated based on Object Keypoint Similarity (OKS):

$$OKS = \frac{\sum_i \exp(-d_i^2/2s^2j_i^2)\sigma(v_i > 0)}{\sum_i \sigma(v_i > 0)} \quad (8)$$

where d_i is the Euclidean distance between the i -th predicted keypoint coordinate and its corresponding coordinate groundtruth, j_i is a constant, v_i is the visibility flag, and s is the object scale.

Baselines. There are many **CNN-based** and recent **Transformer-based** methods for HPE. To show the superiority of the proposed SimDR, we choose two state-of-the-art methods (i.e., SimpleBaseline [37] and HRNet [29]) from the former and one (i.e., TokenPose [17]) from the latter as our baselines.

⁴Label smoothing is adopted to help model training.

Table 2: Comparisons between *heatmap* and the proposed *SimDR* on the COCO validation set, provided with the same detected human boxes. Extra post. = extra post-processing towards refining the predicted keypoint coordinate.

Method	Representation	Input size	#Params	GFLOPs	Extra post.	AP	AR
SimBa-Res50 [37]	heatmap	64×64	34.0M	0.7	Y	34.4	43.7
	heatmap	64×64	34.0M	0.7	N	25.8 (↓8.6)	36.0 (↓7.7)
	SimDR	64×64	34.1M	0.7	N	40.8 (↑6.4)	49.6 (↑5.9)
	heatmap	128×128	34.0M	3.0	Y	60.3	67.6
	heatmap	128×128	34.0M	3.0	N	55.4 (↓4.9)	63.3 (↓4.3)
	SimDR	128×128	34.8M	3.0	N	62.6 (↑2.3)	69.5 (↑1.9)
	heatmap	256×192	34.0M	8.9	Y	70.4	76.3
	heatmap	256×192	34.0M	8.9	N	68.5 (↓1.9)	74.8 (↓1.5)
	SimDR	256×192	36.8M	9.0	N	71.4 (↑1.0)	77.4 (↑1.1)
TokenPose-S [17]	heatmap	64×64	4.9M	1.4	Y	57.1	64.8
	heatmap	64×64	4.9M	1.4	N	35.9 (↓21.2)	47.0 (↓17.8)
	SimDR	64×64	4.9M	1.4	N	62.8 (↑5.7)	70.1 (↑5.3)
	heatmap	128×128	5.2M	1.6	Y	65.4	71.6
	heatmap	128×128	5.2M	1.6	N	57.6 (↓7.8)	64.9 (↓6.7)
	SimDR	128×128	5.1M	1.6	N	70.4 (↑5.0)	76.4 (↑4.8)
	heatmap	256×192	6.6M	2.2	Y	72.5	78.0
	heatmap	256×192	6.6M	2.2	N	69.9 (↓2.6)	75.8 (↓2.2)
	SimDR	256×192	5.5M	2.2	N	73.6 (↑1.1)	78.9 (↑0.9)
SimBa-Res101 [37]	heatmap	64×64	53.0M	1.0	Y	34.1	43.5
	heatmap	64×64	53.0M	1.0	N	25.7 (↓8.4)	36.1 (↓7.4)
	SimDR	64×64	53.1M	1.0	N	39.6 (↑5.5)	48.9 (↑5.4)
	heatmap	128×128	53.0M	4.1	Y	59.2	66.7
	heatmap	128×128	53.0M	4.1	N	54.4 (↓4.8)	62.5 (↓4.2)
	SimDR	128×128	53.5M	4.1	N	63.1 (↑3.9)	70.1 (↑3.4)
	heatmap	256×192	53.0M	12.4	Y	71.4	77.1
	heatmap	256×192	53.0M	12.4	N	69.5 (↓1.9)	75.6 (↓1.5)
	SimDR	256×192	55.7M	12.4	N	72.3 (↑0.9)	78.0 (↑0.9)
HRNet-W32 [29]	heatmap	64×64	28.5M	0.6	Y	45.8	55.3
	heatmap	64×64	28.5M	0.6	N	34.6 (↓11.2)	45.6 (↓9.7)
	SimDR	64×64	28.6M	0.6	N	56.4 (↑10.6)	64.9 (↑9.6)
	heatmap	128×128	28.5M	2.4	Y	67.2	74.1
	heatmap	128×128	28.5M	2.4	N	61.9 (↓5.3)	69.4 (↓4.7)
	SimDR	128×128	29.1M	2.4	N	70.7 (↑3.5)	76.7 (↑2.6)
	heatmap	256×192	28.5M	7.1	Y	74.4	79.8
	heatmap	256×192	28.5M	7.1	N	72.3 (↓2.1)	78.2 (↓1.6)
	SimDR	256×192	31.3M	7.1	N	75.3 (↑0.9)	80.8 (↑1.0)
HRNet-W48 [29]	heatmap	64×64	63.6M	1.2	Y	48.5	57.8
	heatmap	64×64	63.6M	1.2	N	36.9 (↓11.6)	47.8 (↓10.0)
	SimDR	64×64	63.7M	1.2	N	59.7 (↑11.2)	67.5 (↑9.7)
	heatmap	128×128	63.6M	4.9	Y	68.9	75.3
	heatmap	128×128	63.6M	4.9	N	63.3 (↓5.6)	70.5 (↓4.8)
	SimDR	128×128	64.1M	4.9	N	72.0 (↑3.1)	77.9 (↑2.6)
	heatmap	256×192	63.6M	14.6	Y	75.1	80.4
	heatmap	256×192	63.6M	14.6	N	73.1 (↓2.0)	78.7 (↓1.7)
	SimDR	256×192	66.3M	14.6	N	75.9 (↑0.8)	81.2 (↑0.8)

Implementation details. For the selected baselines, we simply follow the original settings in their papers. Specifically, for SimpleBaseline [37], the base learning rate is set as $1e-3$, and is dropped to $1e-4$ and $1e-5$ at the 90-th and 120-th epochs respectively. For HRNet [29], the base learning rate is set as $1e-3$, and decreased to $1e-4$ and $1e-5$ at the 170-th and 200-th epochs. The total training processes are terminated within 140 and 210 epochs respectively for SimpleBaseline [37] and HRNet [29]. Note that the training process of TokenPose-S follows [29].

In this paper, we use the two-stage [29, 37, 5, 26] top-down human pose estimation pipeline: the person instances are firstly detected and then the keypoints are estimated. We adopt a popular person detector with 56.4% AP provided by [37] for COCO validation set. Experiments are conducted in 8 NVIDIA Tesla V100 GPUs.

Table 3: Results with higher input resolutions on the COCO validation set. Different from heatmap-based methods, there is no need of extra post-processing to refine the predicted coordinates for SimDR-based methods. SimDR* is the advanced space-aware variant of SimDR.

Method	Representation	Input size	#Params	GFLOPs	AP	AP ⁵⁰	AP ⁷⁵	AP ^M	AP ^L	AR
HRNet-W48 [29]	heatmap	256×192	63.6M	14.6	75.1	90.6	82.2	71.5	81.8	80.4
	SimDR	256×192	66.3M	14.6	75.9	90.4	82.7	72.4	82.5	81.2
	SimDR*	256×192	66.3M	14.6	76.1 (↑1.0)	90.6	82.9	72.6	82.9	81.2
	heatmap	384×288	63.6M	32.9	76.3	90.8	82.9	72.3	83.4	81.2
	SimDR	384×288	70.6M	32.9	69.9	84.7	75.8	67.3	80.5	78.1
	SimDR*	384×288	70.6M	32.9	76.9 (↑0.6)	90.9	83.2	73.2	83.8	82.0

Table 4: Latency comparisons. Results are achieved on the COCO validation set. ‘Deconv.’ represents the deconvolution module, which can be reserved or directly removed after using SimDR.

Method	Representation	Input size	Deconv.	#Params	GFLOPs	AP	FPS
SimBa-Res50 [37]	heatmap	64×64	Y	34.0M	0.7	34.4	34
	SimDR	64×64	N	24.7M (↓27.4%)	0.3 (↓57.1%)	39.3 (↑4.9)	45 (↑32.4%)
	heatmap	128×128	Y	34.0M	3.0	60.3	21
	SimDR	128×128	N	25.0M (↓26.5%)	1.3 (↓56.7%)	62.6 (↑2.3)	29 (↑38.1%)
	heatmap	256×192	Y	34.0M	8.9	70.4	17
	SimDR	256×192	N	25.7M (↓24.4%)	3.8 (↓57.3%)	70.8 (↑0.4)	21 (↑23.5%)

4.1.1 2D heatmap vs. 1D SimDR

In this part, we give a comprehensive investigation on the superiority of using SimDR as a coordinate representation scheme compared to the heatmap representation. The comparisons are conducted from the perspectives of *complexity*, *performance*, and *speed*.

Representation complexity. Given an image with $H \times W \times 3$ size, heatmap-based methods aim at obtaining a 2D heatmap with size $\frac{H}{\lambda} \times \frac{W}{\lambda}$. Here λ is the downsampling ratio, which is a constant. Hence, the scale complexity of heatmap representation is $O(H \times W)$. Instead, SimDR-based methods aim at yielding two 1D vectors with the size of $H \cdot k$ and $W \cdot k$ respectively. Considering k is a constant, the complexity of SimDR representation is $O(H + W)$, which is much more efficient than heatmap. Particularly, SimDR allows some methods to directly remove the extra independent deconvolution module, resulting in a significant reduction of both model parameters and GFLOPs (see more details in Table 4).

Generality and multiple-resolution robustness. We empirically investigate the generality and robustness (various models & input resolutions) of the proposed SimDR on the COCO validation set. We choose some top-performed CNN-based and Transformer-based methods as our baselines. Table 2 presents the comparisons between the 2D heatmap and the 1D SimDR, showing that the proposed method consistently provides significant performance gains, especially in low-resolution input cases.

Note that different from the heatmap-based methods, SimDR-based methods do not require extra post-processing (e.g., empirical second peak shifting strategy [22]) to improve the accuracy of the predicted joint positions. We here take the state-of-the-art HRNet-W48 [29] as an example to show the superiority of our method. At the input size of 64×64, SimDR outperforms the heatmap-based ones w/ and w/o extra post-processing by 11.2 and 22.8 AP, respectively. And the improvements are 3.1/8.7 AP and 0.8/2.8 AP for the input size of 128×128 and 256×192.

Inference latency analysis. We discuss the impact of our proposed SimDR to the inference latency for SimpleBaseline [37], TokenPose-S [17] and HRNet-W48 [29]. The ‘inference latency’ here refers to the average time consuming of model feedforward (we compute 300 samples with batchsize=1). We adopt FPS to quantitatively illustrate the inference latency. The CPU implementation results are presented with the same machine⁵.

⁵Intel(R) Xeon(R) Gold 6130 CPU @ 2.10GHz

The upsampling module is adopted in SimpleBaseline[37] to obtain 2D heatmap with $\frac{1}{4}$ input resolution size, consisting of three time-consuming deconvolution layers. Due to the use of SimDR as coordinate representation instead of the heatmap, the upsampling module can be removed. Table 4 shows the results of SimpleBaseline on the COCO validation set. We can see that adopting SimDR allows one to remove the costly deconvolution layers of SimpleBaseline. In this way, SimDR contributes 4.9 AP gain with a significant reduction of model parameters and GFLOPs ($\downarrow 27.4\% ; \downarrow 57.1\%$), resulting in 32% faster speed at the input size of 64×64 . Table 4 illustrates that SimDR can consistently reduce the computational cost across various input resolutions.

Due to that SimpleBaseline [37] uses an encoder-decoder architecture, we can replace its decoder part (deconvolutions) with a linear projection head for SimDR. But for HRNet [29] and TokenPose [17], they have no extra independent modules as the decoder. To apply SimDR to them, we directly append an extra linear layer to the original HRNet and replace the MLP head of TokenPose with a linear layer. These are minor changes to the original architectures, thus only bringing a little computation overhead for HRNet [29] and even reducing the computational costs for TokenPose [17] (see the model parameters and GFLOPs in Table 2). Hence, SimDR only has a slight impact on the inference latency for HRNet or TokenPose. For instance, the FPS of HRNet-W48 using heatmap or SimDR is almost the same (4.5/4.8) at the input size of 256×192 .

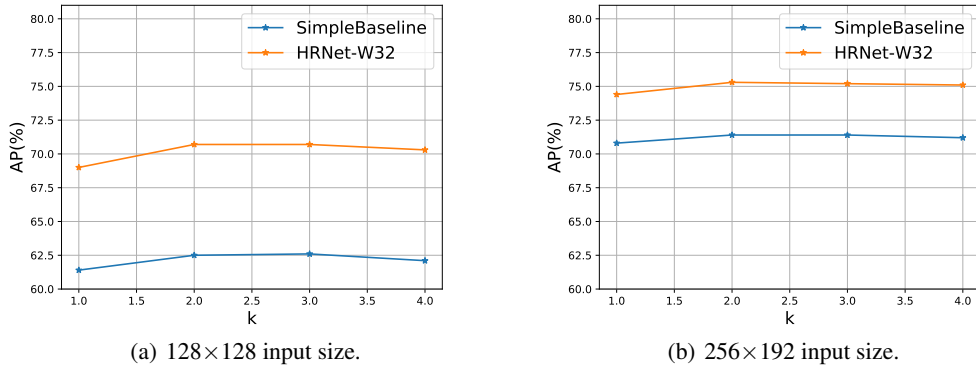


Figure 3: Ablation study of splitting factor k value across various input resolutions. The presented SimpleBaseline [37] uses ResNet-50 as backbone and all results reported are based on the COCO validation set.

4.1.2 Comparison with State-of-the-art Methods

Results on the COCO validation set. We conduct extensive experiments on the COCO validation set for comparing heatmap-based and the proposed SimDR, as shown in Table 2. SimDR shows a consistent performance superiority over heatmap-based ones across various state-of-the-art models and input resolutions, without extra post-processing to refine the predicted keypoint coordinate. One can see more details and discussions by revisiting Section 4.1.1.

Where is the performance boundary of SimDR? To explore the performance boundary of the proposed SimDR and its advanced variant – space-aware SimDR, we compare their results on higher input resolutions, as shown in Table 3. For SimpleBaseline-Res50 [37], SimDR provide 0.8 points gain over heatmap-based representation (see Appendix A for more results). While, for HRNet-W48 [29] at the input size of 384×288 , the naive SimDR causes performance degradation. It illustrates that it is sub-optimal to treat the false labels equally in the naive SimDR, which may cause overfitting for the models with rich capacity at very high input size. As shown in Table 3, we can see that this issue is fixed by the proposed space-aware SimDR that takes the spatial relevance of adjacent labels into consideration. Specifically, SimDR* achieves 0.6 points improvement compared to heatmap-based HRNet-W48 [29] at the input size of 384×288 . The step from naive SimDR towards space-aware SimDR may reveal that there still is further scope to push the performance boundary of SimDR by powering it with more carefully designed loss functions or supervised signals.

Table 5: Results on the COCO test-dev set. ‘Trans.’ represents Transformer [35] for short. ‘Hybrid representation’ represents the methods that simultaneously use the 2D heatmap and absolute coordinate (or offsets, etc.) as the supervision signals.

Method	Encoder	Input size	GFLOPs	AP	AP ⁵⁰	AP ⁷⁵	AP ^M	AP ^L	AR
Heatmap-based									
Mask-RCNN [10]	ResNet-50-FPN	-	-	63.1	87.3	68.7	57.8	71.4	-
CMU-Pose [3]	VGG-19 [28]	-	-	64.2	86.2	70.1	61.0	68.8	-
G-RMI [26]	ResNet-101 [11]	353×257	-	64.9	85.5	71.3	62.3	70.0	69.7
AE [21]	Hourglass [22]	512×512	-	65.5	86.8	72.3	60.6	72.6	70.2
MultiPoseNet [13]	-	480×480	-	69.6	86.3	76.6	65.0	76.3	73.5
RMPE [8]	PyraNet [39]	320×256	26.7	72.3	89.2	79.1	68.0	78.6	-
CPN [5]	ResNet-Inception	384×288	29.2	72.1	91.4	80.0	68.7	77.2	78.5
CFN [12]	-	-	-	72.6	86.1	69.7	78.3	64.1	-
SimBa [37]	ResNet-50	384×288	20.0	71.5	91.1	78.7	67.8	78.0	76.9
SimBa [37]	ResNet-152	384×288	35.6	73.7	91.9	81.1	70.3	80.0	79.0
TransPose-H [38]	HRNet-W48+Trans.	256×192	21.8	75.0	92.2	82.3	71.3	81.1	80.1
HRNet-W32 [29]	HRNet-W32	384×288	16.0	74.9	92.5	82.8	71.3	80.9	80.1
HRNet-W48 [29]	HRNet-W48	256×192	14.6	74.2	92.4	82.4	70.9	79.7	79.5
HRNet-W48 [29]	HRNet-W48	384×288	32.9	75.5	92.5	83.3	71.9	81.5	80.5
Hybrid representation									
Personlab (heatmap+offset map) [25]	ResNet-101	-	-	65.5	87.1	71.4	61.3	71.5	70.1
CenterNet (heatmap+offset map) [41]	Hourglass [22]	-	-	63.0	86.8	69.6	58.9	70.4	-
SPM (heatmap+offset map) [24]	Hourglass [22]	-	-	66.9	88.5	72.9	62.6	73.1	-
DirectPose (heatmap+offset map) [32]	ResNet-50	-	-	62.2	86.4	68.2	56.7	69.8	-
PointSetNet (heatmap+offset map) [36]	HRNet-W48	-	-	68.7	89.9	76.3	64.8	75.3	-
Integral Pose (heatmap+soft-argmax) [31]	ResNet-101	256×256	11.0	67.8	88.2	74.8	63.9	74.0	-
DEKR (heatmap+offset map) [9]	HRNet-W48	640×640	-	72.3	88.3	78.6	68.6	78.6	77.7
TFPose (heatmap+coordinate) [20]	ResNet-50+Trans.	384×288	20.4	72.2	90.9	80.1	69.1	78.8	-
Heatmap-free									
DeepPose [34]	ResNet-101	256×192	7.7	57.4	86.5	64.2	55.0	62.8	-
DeepPose [34]	ResNet-152	256×192	11.3	59.3	87.6	66.7	56.8	64.9	-
PRTR [15]	HRNet-W48+Trans.	-	-	64.9	87.0	71.7	60.2	72.5	74.1
PRTR [15]	HRNet-W32+Trans.	384×288	21.6	71.7	90.6	79.6	67.6	78.4	78.8
PRTR [15]	HRNet-W32+Trans.	512×384	37.8	72.1	90.4	79.6	68.1	79.0	79.4
SimBa (SimDR*)	ResNet-50	384×288	20.2	72.7	91.2	80.1	69.2	79.0	78.0
HRNet (SimDR*)	HRNet-W48	256×192	14.6	75.4	92.4	82.7	71.9	81.3	80.5
HRNet (SimDR*)	HRNet-W48	384×288	32.9	76.0	92.4	83.5	72.5	81.9	81.1

Results on the COCO test-dev set. We report the results of our method and other state-of-the-art methods in Table 5. Based on the degree of reliance on heatmap, we further divide existing approaches into *heatmap-based*, *hybrid representation*, and *heatmap-free* methods. The methods [25, 24, 32, 36, 9, 20] that simultaneously use the heatmap and coordinate (or offsets, etc.) representations as the supervision signals are regarded as the ‘hybrid representation’ methods.

The results in Table 5 shows that the gap between heatmap-based and heatmap-free methods has been closed by the proposed SimDR for the first time. Specifically, as a kind of heatmap-free method, SimDR* achieves 76.0 AP at the input size 384×288, outperforming PRTR [15] by a large margin (↑3.9). In addition, even compared with heatmap-based counterpart, SimDR* still shows 0.5 points improvement at the input size of 384×288.

4.2 Ablation Study

Analysis on the splitting factor k . Recalling Section 3.2, there is only one hyperparameter when optimizing SimDR, *i.e.*, the splitting factor k . We point out that k controls the sub-pixel accuracy level of the joint location in SimDR. Specifically, the larger k is, the smaller the quantization error of SimDR is. Nevertheless, model training becomes more difficult when k increases. Hence, there is a trade-off between the quantisation error and the model performance.

We test $k \in \{1, 2, 3, 4\}$ based on SimpleBaseline [37] and HRNet [29] under various input resolutions. As shown in Figure 3, model performance tends to increase first and then decrease as k grows. For HRNet-W32 [29], the recommended settings are $k = 2$ for both 128×128 and 256×192 input size. For SimBa-Res50 [37], the recommended settings are $k = 3$ and $k = 2$ for 128×128 and 256×192 input size, respectively.

5 Discussion

SimDR allows one to directly remove the time-consuming upsampling module of some methods, which may induce lightweight architectures for HPE. Our extensive experiments on various neural networks also reflect that a pose estimation model can be seen as two parts: an encoder to learn good embeddings and a head to transform embeddings into keypoint coordinate encodings. This may encourage future researches to explore more efficient designs of neural network as the encoder and more potential coordinate encoding schemes.

For another direction - applying SimDR to bottom-up multi-person pose estimation, the presence of multiple people brings the identification ambiguity in decoding joint candidate positions from two disentangled vectors. It is likely that future works can introduce new dimensions beyond x and y dimensions to address this issue.

6 Conclusion

In this paper, we explore a simple yet promising coordinate representation (namely SimDR). It disentangles the x - and y - coordinate of joint location into two independent 1D vectors, regarding the keypoint localization task as two sub-tasks of classification at horizontal and vertical directions. The experimental results empirically show that the 2D structure might not be a key ingredient for coordinate representation to sustain superior performance. The proposed SimDR shows advantages over heatmap-based representation at model performances and the simplicity of post-processing steps. Moreover, it may also inspire new works on lightweight model design for HPE. We demonstrate that SimDR can be easily integrated with any common CNN-based or Transformer-based neural networks. Comprehensive experiments illustrate that the proposed SimDR is generic and consistently outperforms the heatmap-based counterparts in all cases, especially in low input resolutions.

References

- [1] Mykhaylo Andriluka, Leonid Pishchulin, Peter Gehler, and Bernt Schiele. 2d human pose estimation: New benchmark and state of the art analysis. In *Proceedings of the IEEE Conference on computer Vision and Pattern Recognition*, pages 3686–3693, 2014. [2](#), [5](#), [13](#)
- [2] Yuanhao Cai, Zhicheng Wang, Zhengxiong Luo, Binyi Yin, Angang Du, Haoqian Wang, Xiangyu Zhang, Xinyu Zhou, Erjin Zhou, and Jian Sun. Learning delicate local representations for multi-person pose estimation. In *European Conference on Computer Vision*, pages 455–472. Springer, 2020. [1](#), [3](#)
- [3] Zhe Cao, Gines Hidalgo, Tomas Simon, Shih-En Wei, and Yaser Sheikh. Openpose: realtime multi-person 2d pose estimation using part affinity fields. *IEEE transactions on pattern analysis and machine intelligence*, 43(1):172–186, 2019. [1](#), [3](#), [9](#)
- [4] Joao Carreira, Pulkit Agrawal, Katerina Fragkiadaki, and Jitendra Malik. Human pose estimation with iterative error feedback. In *Proceedings of the IEEE conference on computer vision and pattern recognition*, pages 4733–4742, 2016. [3](#)
- [5] Yilun Chen, Zhicheng Wang, Yuxiang Peng, Zhiqiang Zhang, Gang Yu, and Jian Sun. Cascaded pyramid network for multi-person pose estimation. In *Proceedings of the IEEE conference on computer vision and pattern recognition*, pages 7103–7112, 2018. [1](#), [3](#), [6](#), [9](#)
- [6] Bowen Cheng, Bin Xiao, Jingdong Wang, Honghui Shi, Thomas S Huang, and Lei Zhang. Higherhrnet: Scale-aware representation learning for bottom-up human pose estimation. In *Proceedings of the IEEE/CVF Conference on Computer Vision and Pattern Recognition*, pages 5386–5395, 2020. [1](#), [3](#)
- [7] Matteo Fabbri, Fabio Lanzi, Simone Calderara, Stefano Alletto, and Rita Cucchiara. Compressed volumetric heatmaps for multi-person 3d pose estimation. In *Proceedings of the IEEE/CVF Conference on Computer Vision and Pattern Recognition*, pages 7204–7213, 2020. [2](#)
- [8] Hao-Shu Fang, Shuqin Xie, Yu-Wing Tai, and Cewu Lu. Rmpe: Regional multi-person pose estimation. In *Proceedings of the IEEE International Conference on Computer Vision*, pages 2334–2343, 2017. [9](#)
- [9] Zigang Geng, Ke Sun, Bin Xiao, Zhaoxiang Zhang, and Jingdong Wang. Bottom-up human pose estimation via disentangled keypoint regression. *arXiv preprint arXiv:2104.02300*, 2021. [9](#)
- [10] Kaiming He, Georgia Gkioxari, Piotr Dollár, and Ross Girshick. Mask r-cnn. In *Proceedings of the IEEE international conference on computer vision*, pages 2961–2969, 2017. [9](#)
- [11] Kaiming He, Xiangyu Zhang, Shaoqing Ren, and Jian Sun. Deep residual learning for image recognition. In *Proceedings of the IEEE conference on computer vision and pattern recognition*, pages 770–778, 2016. [9](#)
- [12] Shaoli Huang, Mingming Gong, and Dacheng Tao. A coarse-fine network for keypoint localization. In *Proceedings of the IEEE International Conference on Computer Vision*, pages 3028–3037, 2017. [9](#)

[13] Muhammed Kocabas, Salih Karagoz, and Emre Akbas. Multiposenet: Fast multi-person pose estimation using pose residual network. In *Proceedings of the European conference on computer vision (ECCV)*, pages 417–433, 2018. 9

[14] Jiefeng Li, Can Wang, Hao Zhu, Yihuan Mao, Hao-Shu Fang, and Cewu Lu. Crowdpose: Efficient crowded scenes pose estimation and a new benchmark. In *Proceedings of the IEEE/CVF Conference on Computer Vision and Pattern Recognition*, pages 10863–10872, 2019. 2, 5, 13

[15] Ke Li, Shijie Wang, Xiang Zhang, Yifan Xu, Weijian Xu, and Zhuowen Tu. Pose recognition with cascade transformers. *arXiv preprint arXiv:2104.06976*, 2021. 1, 3, 9

[16] Wenbo Li, Zhicheng Wang, Binyi Yin, Qixiang Peng, Yuming Du, Tianzi Xiao, Gang Yu, Hongtao Lu, Yichen Wei, and Jian Sun. Rethinking on multi-stage networks for human pose estimation. *arXiv preprint arXiv:1901.00148*, 2019. 1, 3

[17] Yanjie Li, Shoukui Zhang, Zhicheng Wang, Sen Yang, Wankou Yang, Shu-Tao Xia, and Erjin Zhou. Tokenpose: Learning keypoint tokens for human pose estimation. *arXiv preprint arXiv:2104.03516*, 2021. 1, 2, 3, 5, 6, 7, 8

[18] Tsung-Yi Lin, Michael Maire, Serge Belongie, James Hays, Pietro Perona, Deva Ramanan, Piotr Dollár, and C Lawrence Zitnick. Microsoft coco: Common objects in context. In *European conference on computer vision*, pages 740–755. Springer, 2014. 2, 5, 13

[19] Zhengxiong Luo, Zhicheng Wang, Yan Huang, Tieniu Tan, and Erjin Zhou. Rethinking the heatmap regression for bottom-up human pose estimation. *arXiv preprint arXiv:2012.15175*, 2020. 1, 3

[20] Weian Mao, Yongtao Ge, Chunhua Shen, Zhi Tian, Xinlong Wang, and Zhibin Wang. Tfpose: Direct human pose estimation with transformers. *arXiv preprint arXiv:2103.15320*, 2021. 1, 3, 9

[21] Alejandro Newell, Zhiao Huang, and Jia Deng. Associative embedding: End-to-end learning for joint detection and grouping. In *Advances in Neural Information Processing Systems*, 2017. 9

[22] Alejandro Newell, Kaiyu Yang, and Jia Deng. Stacked hourglass networks for human pose estimation. In *European conference on computer vision*, pages 483–499. Springer, 2016. 1, 3, 7, 9

[23] Aiden Nibali, Zhen He, Stuart Morgan, and Luke Prendergast. Numerical coordinate regression with convolutional neural networks. *arXiv preprint arXiv:1801.07372*, 2018. 3

[24] Xuecheng Nie, Jiashi Feng, Jianfeng Zhang, and Shuicheng Yan. Single-stage multi-person pose machines. In *Proceedings of the IEEE/CVF International Conference on Computer Vision*, pages 6951–6960, 2019. 3, 9

[25] George Papandreou, Tyler Zhu, Liang-Chieh Chen, Spyros Gidaris, Jonathan Tompson, and Kevin Murphy. Personlab: Person pose estimation and instance segmentation with a bottom-up, part-based, geometric embedding model. In *Proceedings of the European Conference on Computer Vision*, pages 269–286, 2018. 9

[26] George Papandreou, Tyler Zhu, Nori Kanazawa, Alexander Toshev, Jonathan Tompson, Chris Bregler, and Kevin Murphy. Towards accurate multi-person pose estimation in the wild. In *Proceedings of the IEEE Conference on Computer Vision and Pattern Recognition*, pages 4903–4911, 2017. 3, 6, 9

[27] Joseph Redmon and Ali Farhadi. Yolov3: An incremental improvement. *arXiv preprint arXiv:1804.02767*, 2018. 13

[28] Karen Simonyan and Andrew Zisserman. Very deep convolutional networks for large-scale image recognition. *arXiv preprint arXiv:1409.1556*, 2014. 9

[29] Ke Sun, Bin Xiao, Dong Liu, and Jingdong Wang. Deep high-resolution representation learning for human pose estimation. In *Proceedings of the IEEE/CVF Conference on Computer Vision and Pattern Recognition*, pages 5693–5703, 2019. 1, 2, 3, 5, 6, 7, 8, 9, 13, 14

[30] Xiao Sun, Jiaxiang Shang, Shuang Liang, and Yichen Wei. Compositional human pose regression. In *Proceedings of the IEEE International Conference on Computer Vision*, pages 2602–2611, 2017. 3

[31] Xiao Sun, Bin Xiao, Fangyin Wei, Shuang Liang, and Yichen Wei. Integral human pose regression. In *Proceedings of the European Conference on Computer Vision*, pages 529–545, 2018. 1, 3, 9

[32] Zhi Tian, Hao Chen, and Chunhua Shen. Directpose: Direct end-to-end multi-person pose estimation. *arXiv preprint arXiv:1911.07451*, 2019. 1, 3, 9

[33] Jonathan Tompson, Arjun Jain, Yann LeCun, and Christoph Bregler. Joint training of a convolutional network and a graphical model for human pose estimation. *arXiv preprint arXiv:1406.2984*, 2014. 3

[34] Alexander Toshev and Christian Szegedy. Deeppose: Human pose estimation via deep neural networks. In *Proceedings of the IEEE conference on computer vision and pattern recognition*, pages 1653–1660, 2014. 1, 3, 9

[35] Ashish Vaswani, Noam Shazeer, Niki Parmar, Jakob Uszkoreit, Llion Jones, Aidan N Gomez, Łukasz Kaiser, and Illia Polosukhin. Attention is all you need. *arXiv preprint arXiv:1706.03762*, 2017. 9

[36] Fangyun Wei, Xiao Sun, Hongyang Li, Jingdong Wang, and Stephen Lin. Point-set anchors for object detection, instance segmentation and pose estimation. In *European Conference on Computer Vision*, pages 527–544. Springer, 2020. 9

[37] Bin Xiao, Haiping Wu, and Yichen Wei. Simple baselines for human pose estimation and tracking. In *Proceedings of the European conference on computer vision*, pages 466–481, 2018. 1, 2, 3, 5, 6, 7, 8, 9, 13

- [38] Sen Yang, Zhibin Quan, Mu Nie, and Wankou Yang. Transpose: Towards explainable human pose estimation by transformer. *arXiv preprint arXiv:2012.14214*, 2020. [1](#), [2](#), [3](#), [9](#)
- [39] Wei Yang, Shuang Li, Wanli Ouyang, Hongsheng Li, and Xiaogang Wang. Learning feature pyramids for human pose estimation. In *proceedings of the IEEE international conference on computer vision*, pages 1281–1290, 2017. [9](#)
- [40] Feng Zhang, Xiatian Zhu, Hanbin Dai, Mao Ye, and Ce Zhu. Distribution-aware coordinate representation for human pose estimation. In *Proceedings of the IEEE/CVF conference on computer vision and pattern recognition*, pages 7093–7102, 2020. [1](#), [3](#), [15](#)
- [41] Xingyi Zhou, Dequan Wang, and Philipp Krähenbühl. Objects as points. *arXiv preprint arXiv:1904.07850*, 2019. [9](#)

A Results on Higher Input Resolution

SimDR-based methods have shown huge superiority compared to heatmap-based counterparts at low input resolutions (e.g., 64×64). Moreover, we argue that even at very high input resolutions, SimDR-based methods still achieve competitive performance to heatmap-based counterparts. We present the comparisons between heatmap-based and SimDR-based SimpleBaseline [37] at the input size of 384×288 in Table 6.

Table 6: Results on the COCO validation set with the input size of 384×288 .

Method	Representation	AP	AP ⁵⁰	AP ⁷⁵	AP ^M	AP ^L	AR
SimBa-Res50 [37]	heatmap	72.2	89.3	78.9	68.1	79.7	77.6
	SimDR	73.0 ($\uparrow 0.8$)	89.3	79.7	69.5	79.9	78.6
SimBa-Res101 [37]	heatmap	73.6	89.6	80.3	69.9	81.1	79.1
	SimDR	74.2 ($\uparrow 0.6$)	89.6	80.9	70.7	80.9	79.8
SimBa-Res152 [37]	heatmap	74.3	89.6	81.1	70.5	81.6	79.7
	SimDR	74.9 ($\uparrow 0.6$)	89.9	81.5	71.4	81.7	80.4

B Results on CrowdPose

We further illustrate the effectiveness of the proposed SimDR on the CrowdPose [14] dataset, which contains much more crowded scenes than the COCO keypoint dataset. There are 20,000 images and 80,000 person instances in the CrowdPose. The training, validation and testing subset consist of about 10,000, 2,000, and 8,000 images respectively. Similar evaluation metric to that of COCO [18] is adopted here, with extra AP^E (AP scores on relatively easier samples) and AP^H (AP scores on harder samples). We follow the original paper [14] to adopt YoloV3 [27] as the human detector, and batch size is set as 64.

We compare SimDR-based methods with the heatmap-based counterparts on the CrowdPose test dataset, at the input size of 64×64 and 256×192 respectively. The results in Table 7 show that SimDR-based ones outperform heatmap-based methods by a large margin at the input resolution of 64×64 .

Table 7: Results on the CrowdPose test dataset.

Method	Representation	Input size	AP	AP ⁵⁰	AP ⁷⁵	AP ^E	AP ^M	AP ^H
HRNet-W32 [29]	heatmap	64×64	42.4	69.6	45.5	51.2	43.1	31.8
	SimDR	64×64	46.5	70.9	50.0	56.0	47.5	34.7
	heatmap	256×192	66.4	81.1	71.5	74.0	67.4	55.6
	SimDR	256×192	66.7	82.1	72.0	74.1	67.8	56.2

C Results on MPII Human Pose Estimation

The MPII Human Pose dataset [1] contains 40k person samples with 16 joints labels. We point out that the data augmentation used on the MPII dataset is the same as that on the COCO dataset. Additionally, the input images are cropped to 256×256 and 64×64 .

Results on the validation set. We follow the testing procedure in HRNet [29]. The head-normalized probability of correct keypoint (PCKh) [1] score is used for model evaluation. The results are presented in Table 8. SimDR-based ones achieve better performances under the stricter measurement PCKh@0.1.

Table 8: Results on the MPII validation set.

Method	Representation	Input size	Hea	Sho	Elb	Wri	Hip	Kne	Ank	Mean
PCKh@0.5										
HRNet-W32 [29]	heatmap	64×64	89.7	86.6	75.1	65.7	77.2	69.2	63.6	76.4
	SimDR	64×64	93.5	89.5	77.5	67.6	79.8	71.5	65.0	78.7
	heatmap	256×256	97.1	95.9	90.3	86.4	89.1	87.1	83.3	90.3
	SimDR	256×256	96.8	95.9	90.0	85.0	89.1	85.4	81.3	89.6
	SimDR*	256×256	97.2	96.0	90.4	85.6	89.5	85.8	81.8	90.0
	PCKh@0.1									
HRNet-W32 [29]	heatmap	64×64	12.9	11.7	9.7	7.1	7.2	7.2	6.6	9.2
	SimDR	64×64	30.9	23.3	18.1	15.0	10.5	13.1	12.8	18.5
	heatmap	256×256	44.5	37.3	37.5	36.9	15.1	25.9	27.2	33.1
	SimDR	256×256	50.1	41.0	45.3	42.4	16.6	29.7	30.3	37.8
	SimDR*	256×256	49.6	41.9	43.0	39.6	17.0	28.2	28.9	36.8

D Analysis on the Quantisation Error

Given an input image of size $H \times W \times 3$, the ground-truth coordinate for a given keypoint is denoted as (x_{real}, y_{real}) . Here we take the abscissa x_{real} as an example to analyze the quantization error of coordinate encoding.

D.1 SimDR-based Representation

For SimDR, we suppose x_{real} can be rewritten as:

$$x_{real} = \frac{n_s + z_s}{k} = \frac{n_s}{k} + \sigma_s, \quad (9)$$

where $k \geq 1$ is the splitting factor of SimDR, $n_s \in \mathbb{N}$, $0 \leq z_s < 1$ and $0 \leq \sigma_s < \frac{1}{k}$. The ground-truth abscissa is then rescaled by the splitting factor k into a new one :

$$x_s = \text{round}(x_{real} \cdot k) = n_s + \text{round}(\sigma_s \cdot k) = \begin{cases} n_s, & 0 \leq \sigma_s < \frac{1}{2k} \\ n_s + 1, & \frac{1}{2k} \leq \sigma_s < \frac{1}{k} \end{cases} \quad (10)$$

The quantisation error $|\Delta_s|$ is calculated as:

$$|\Delta_s| = \left| \frac{x_s}{k} - x_{real} \right| = \begin{cases} \left| \frac{n_s}{k} - \frac{n_s}{k} - \sigma_s \right|, & 0 \leq \sigma_s < \frac{1}{2k} \\ \left| \frac{n_s+1}{k} - \frac{n_s}{k} - \sigma_s \right|, & \frac{1}{2k} \leq \sigma_s < \frac{1}{k} \end{cases} \quad (11)$$

Therefore, the quantisation error $|\Delta_s|$ of SimDR satisfies: $0 \leq |\Delta_s| < \frac{1}{2k}$.

D.2 Heatmap-based Representation

In this part, we give an analysis for the quantisation error of coordinate encoding of heatmaps generated by following [29]. x_{real} can be rewritten as:

$$x_{real} = n_h \cdot \lambda + \sigma_h \quad (12)$$

where λ is the downsampling ratio, $n_h \in \mathbb{N}$, $0 \leq \sigma_h < \lambda$. Considering the computational cost, the resolution of heatmap is usually downsampled from that of the original input image. Hence, x_{real} is transformed to:

$$x_h = \text{round}\left(\frac{x_{real}}{\lambda}\right) = n_h + \text{round}\left(\frac{\sigma_h}{\lambda}\right) = \begin{cases} n_h, & 0 \leq \sigma_h < \frac{\lambda}{2} \\ n_h + 1, & \frac{\lambda}{2} \leq \sigma_h < \lambda \end{cases} \quad (13)$$

The quantisation error $|\Delta_h|$ can be calculated as:

$$|\Delta_h| = |x_h \cdot \lambda - x_{real}| = \begin{cases} |\sigma_h|, & 0 \leq \sigma_h < \frac{\lambda}{2} \\ |\lambda - \sigma_h|, & \frac{\lambda}{2} \leq \sigma_h < \lambda \end{cases} \quad (14)$$

Based on the discussions above, one can see that: $0 \leq |\Delta_h| < \frac{\lambda}{2}$.

To alleviate the quantisation error of heatmap-based representation, extra post-processing is usually required (e.g., empirical second peak shifting strategy). Moreover, [40] uses more complicated and time-consuming post-processing module to handle this issue. Different from that, SimDR gets rid of extra coordinate refinement and reduces the quantisation error by the coordinate representation design, which is simple and efficient.